

Dynamics from quantum Monte Carlo simulations and the unduly constraining entropic prior

Olav F. Syljuåsen¹

¹*NORDITA, Blegdamsvej 17, DK-2100 Copenhagen Ø, Denmark*

(Dated: February 6, 2020)

The MaxEnt method is often employed to obtain real time dynamics from quantum Monte Carlo simulations. It is argued here that the specific MaxEnt form of the prior probability distribution of spectral functions is inappropriate. This is because it is based on dubious assumptions such as the existence of finite discrete units of spectral weight, or on the interpretation of the spectral function as a one dimensional probability distribution. It is furthermore argued that the MaxEnt prior does not reflect reasonable a priori knowledge about spectral functions and constrains them unduly. Instead we argue in favor of the Average Spectrum Method which samples the posterior probability distribution directly with a less constraining prior. We show several examples of its use. We consider the temperature dependence and broadening of the Haldane gap in a spin-1 antiferromagnetic chain, the dynamic structure factor of the bond alternating spin-1/2 Heisenberg chain with and without a magnetic field, and line shapes of zone boundary excitations of the two dimensional spin-1/2 Heisenberg antiferromagnet.

PACS numbers: 75.40.Gb, 05.10.Ln, 02.50.Tt, 75.10.Jm

I. INTRODUCTION

Quantum Monte Carlo simulations (QMC) has become the method of choice for studying large equilibrium quantum many-body systems without approximations. While thermodynamic and static properties are easily obtained with QMC, obtaining dynamics is more difficult. The reason is that QMC is invariably formulated in *imaginary* instead of real time. This is not just a matter of choice, in fact the imaginary time formulation is necessary to avoid crucial sign problems which would ruin the statistical accuracy of the method. The difficulty in obtaining the dynamics lies in transforming imaginary time correlation functions back to real time. This “Wick rotation” is easily carried out when an *analytic* expression of the imaginary time correlation function is known. However, when only numerical data and their associated error bars are available, as in QMC, it is well known that the direct transformation is ill-defined and very sensitive to the errors.

The common way to deal with this problem is to employ Bayesian statistics which aims at identifying probabilities for different spectral functions that can account for the observed imaginary time data. In finding the best spectral function it is important that the spectral function not only fits the data well, but also that it is consistent with prior knowledge about which types of spectral functions are permissible. The Bayesian statistical framework is well suited for this as both prior knowledge and data-fitting is taken into account.

Although not often coined in the Bayesian language, the procedure of fitting certain specific functional forms to the imaginary time data, is an example of Bayesian analysis where the prior probability distribution assigns equal probabilities to spectral functions of the specific functional form and the fitting procedure selects the best functional parameters. However, fitting to a certain class

of functions assumes a rather high degree of prior knowledge. While such knowledge should be used whenever available it is not so common that one actually knows the exact functional form of the spectral function a priori.

In fact it is more often the case that one does not know the actual shape of the spectral function, but only knows certain sum rules and physical requirements such as real-valuedness and positivity. One should then prefer a prior probability distribution that takes only into account the prior knowledge and do not make extra assumptions. Such a maximally non-committal prior probability distribution is gotten by maximizing the entropy of the distribution under constraints coming from the specific a priori knowledge^{1,2}. In carrying out such a maximization it is important to consider the correct space to perform it in. A probability distribution of spectral functions is clearly multidimensional. Yet it is customary, in the widely popular MaxEnt method^{3,4}, to treat the spectral function itself as a one dimensional probability distribution and choose a prior probability distribution that gives a high probability to spectral functions having a large entropy. Thus instead of maximizing the entropy of the multidimensional probability distribution of spectral functions, the entropy of the spectral function itself is maximized. The latter does not yield the maximally non-committal probability distribution for spectral functions, and in fact unduly constrains the spectral functions to be smooth.

We will in this article argue in favor of another method, the Average Spectrum Method⁵, where the posterior probability distribution is sampled directly using a much less constraining prior. This is also the same idea as used in the Stochastic continuation method proposed in Ref. 6.

This article is structured as follows: In sections II the Bayesian method is discussed. Section III contains discussions of the entropic prior used in the MaxEnt method and its application to the specific problem of concern

here. A less constraining prior is presented in Section IV. The Average Spectrum Method is explained in Section V, and the particular Monte Carlo implementation of it used in this article is described in Section VI. In section VII the Average Spectrum Method is applied to several different quantum spin systems, and the article ends with a summary.

II. BAYESIAN METHOD

The equilibrium dynamics of a physical system is characterized by the spectral function $A(\omega)$ which is real and non-negative. However, in QMC what is typically obtained is an imaginary time correlation function $G(\tau)$ which is related to the spectral function as

$$G(\tau) = \int d\omega K(\tau, \omega) A(\omega) \quad (1)$$

where the kernel of the transform, $K(\tau, \omega)$, takes on different forms depending on whether the operators in the measured correlation function are fermionic or bosonic. In order to make the discussion definite and practical we will model the spectral function as a collection of N delta-functions on a regularly spaced frequency grid ω_i

$$A(\omega) = \sum_{i=1}^N A_{\omega_i} \delta(\omega - \omega_i), \quad (2)$$

where all A_{ω_i} are positive or zero. Furthermore we will assume that $G(\tau)$ is obtained in QMC simulations at discrete imaginary times τ . With this Eq. (1) takes the form

$$G_\tau = \sum_i K_{\tau, \omega_i} A_{\omega_i}. \quad (3)$$

The goal is to invert this relation. However, this inversion is an ill-posed problem because of the near-zero eigenvalues of the kernel and therefore very sensitive to statistical errors of G_τ .

In the Bayesian approach one instead attempts to find the *probability* of a particular spectral function A given the QMC imaginary data G and prior knowledge. This, *posterior* probability $P(A|G)$, can be expressed using Bayes theorem as

$$P(A|G) \propto P(G|A)P(A) \quad (4)$$

where $P(G|A)$ is the likelihood that the QMC data turns out to be G given a particular spectral function A , and $P(A)$ is the prior probability distribution of the spectral function. The prior probability distribution encodes the knowledge we have about the spectral function A before any QMC data is obtained.

III. ENTROPIC PRIOR

In the MaxEnt method the choice of prior probability distribution is the so called entropic prior

$$P(A) \propto e^{-\kappa S}, \quad S = - \sum_i A_{\omega_i} \log A_{\omega_i}, \quad (5)$$

where S is the entropy of the spectral function $A(\omega)$ and κ is a constant.

One may legitimately ask what are the prior knowledge or assumptions that lead to this expression. The common argument justifying it, first used in image restoration⁷, is to imagine monkeys throwing little chunks of spectral weights into bins centered at the frequencies ω_i . In each throw the chunk of spectral weight may land in any of the bins with equal probability. Thus when the monkeys have thrown M chunks such that the total spectral weight corresponds to a prior known sum-rule, they stop, and the spectral weight at frequency ω_i is recorded as the relative number of all frequency chunks that has landed in the bin centered on ω_i . Because the sequence of individual throws leading to a certain spectral function are exchangeable, one can assign a probability to the spectral function by counting in how many ways, denoted by W , it can be realized. With m_i denoting the number of frequency chunks in bin i this number corresponds to the entropic prior Eq. (5) and is

$$W = \frac{M!}{m_1! m_2! \dots m_N!} \approx \exp \left[-M \sum_i A_{\omega_i} \log A_{\omega_i} \right]. \quad (6)$$

where $A_{\omega_i} = m_i/M$. In the last equality we have used Stirling's formula and neglected $1/M$ terms.

However, the picture of monkeys throwing discrete chunks of spectral weights at random does not seem to be very appropriate in describing how nature produces spectral functions. The spectral function is a property of the Hamiltonian of a physical system, and as such it is indivisible. In particular we have no prior knowledge indicating the existence of the discrete units of spectral weights⁸. Once the Hamiltonian is specified the strength of all the different frequency components are in principle determined, thus the monkey building up procedure is inappropriate.

It might be argued, as is often done⁹, that Eq. (5) can also be justified entirely without using the notion of monkeys. From information theory it is known that the probability distribution which satisfies the prior knowledge and assumes the least amount of additional information, the so called maximally non-committal probability distribution, is the one that maximizes the entropy under the constraints given by the prior knowledge. If one interprets the spectral function itself as a probability distribution in one variable ω , then Eq. (5) expresses exactly this, that the entropic prior gives highest likelihood

to probability distributions (spectral functions) having largest entropies. However, although $A(\omega)$ is positive and normalizable, it is *not* a probability distribution in one variable. At least we have no reasonable prior knowledge telling us that the spectral function itself is a probability distribution. The spectral function does not represent the probability of an outcome at a certain frequency, and in particular, a flat spectral function does not represent our ignorance about peak positions, but a Hamiltonian having equal responses to all frequencies. Thus the interpretation of the spectral function as a probability distribution in one variable is an extra assumed prior knowledge of questionable validity.

Without QMC data the most likely spectrum, according to the entropic prior Eq. (5), is the uniform spectrum. Does that conform to our a priori expectations? If we restrict the attention to spectra obtained from QMC simulations of lattice model Hamiltonians the answer is very likely no. For such we do expect to see gaps where the spectral weight is zero, as well as sharp peaks and edges. We might not know exactly at which frequencies these features occur, but we know that they are common, and if they weren't we would probably not perform simulations of such Hamiltonians in the first place.

The entropic prior Eq. (5) can however be generalized to the expression $S = -\sum_i A_{\omega_i} \log(A_{\omega_i}/r_{\omega_i})$ to accommodate for more detailed prior information specified by a function r_{ω} . It is known that the use of such a function can improve the method considerably⁹. However, it can often be quite difficult to determine r_{ω} , and in practice r_{ω} is determined by an adaptive strategy, where one first analyzes the data using a flat prior ($r_{\omega} = 1$), and then take the obtained result to guess a form of r_{ω} which is fed back as a new prior to reanalyze the data. The danger with this procedure is that it blurs the distinction between the prior knowledge and the data. Errors in the data material can clearly be exaggerated if the prior also includes erroneous features. Thus one can easily be led astray if sufficient precautions is not taken to base r_{ω} on firm prior knowledge.

Another example illustrating how little the entropic prior reflects prior knowledge about the spectral function is the frequent use of the single-mode approximation in analyzing QMC data. In this approximation all the spectral weight is assumed to be located in a single delta-function. Such a delta-function assumption about the spectrum has a very low probability according to Eq. (5), as such a spectral function corresponds to the one with the *smallest* entropy.

While the entropic prior Eq. (5) does not seem to reflect our prior knowledge there is nothing wrong with the maximum entropy principle itself. The issue is rather whether one maximizes the entropy of a one-dimensional or a multi-dimensional probability distribution. In order to illustrate this consider for simplicity a physical system with only two frequencies ω_1 and ω_2 . Thus the spectral function is completely specified by the two numbers $(A_{\omega_1}, A_{\omega_2})$. Furthermore, again for simplicity, let

		A_{ω_2}		
		0	1	2
A_{ω_1}	0	0	0	y
	1	0	$1-x-y$	0
	2	x	0	0

TABLE I: Probability table for the occurrence of a spectral function A in the simple case where it only has two frequencies with three possible values each. x and y are restricted so that all entries of the table are non-negative, and the zeros is a consequence of the sum-rule described in the text.

each A_{ω} take one out of three integer values in the range $\{0, 1, 2\}$, thus giving a total of nine possible spectral functions. Let us also assume that it is known from a sum-rule that $A_{\omega_1} + A_{\omega_2} = 2$. This represents our prior knowledge. The prior knowledge restricts the possible solutions to only three spectral functions as only $(2, 0)$, $(1, 1)$ and $(0, 2)$ fulfill the sum rule. However, there is no a priori reason to favor any particular one of these three. Yet maximizing the entropy $-A_{\omega_1} \log A_{\omega_1} - A_{\omega_2} \log A_{\omega_2}$ subject to the constraint $A_{\omega_1} + A_{\omega_2} = 2$ gives $(1, 1)$, the flat spectrum, as the solution with highest probability and $(2, 0)$ and $(0, 2)$ with lower probabilities. However, if one instead assigns probabilities to each spectral function, so that the probability distribution is a function of, here two, but in general as many variables as there are frequencies, one arrives at the Table I. Maximizing the entropy $-x \log x - y \log y - (1-x-y) \log(1-x-y)$ where the sum-rule has already been taken into account in constructing the table, one obtains $x = y = 1/3$. That is the spectral functions $(2, 0)$, $(1, 1)$ and $(0, 2)$ are equally likely, thus the “multidimensional” entropic prior assigns equal probabilities to these, as is what one would naturally describe as the noncommittal probability assignment.

IV. A LESS CONSTRAINING PRIOR

From the arguments in the previous section it follows that it is desirable to replace Eq. (5) with an expression that better corresponds to our prior knowledge about spectral functions. By generalizing the example shown in Table I we suggest to use

$$P(A) \propto \delta\left(\sum_i K_{0\omega_i} A_{\omega_i} - G_0\right) \prod_i \Theta(A_{\omega_i}) \quad (7)$$

as a prior probability distribution. Here $\Theta(x) = 1$ for $x \geq 0$ and zero otherwise. The product of Θ -functions incorporates the knowledge that all spectral components must be non-negative, and the δ -function constrains the spectra to obey a zero-moment sum rule. Higher order sum rules can be implemented by multiplying by more δ -functions. This prior probability distribution is flatter, or less selective, than Eq. (5), as no selection is made between two positive spectra that obey the sum rule. Thus in contrast to the MaxEnt method which naturally selects a unique best spectrum; the smoothest spectrum

among those that best fit the data, the Eq. (7) will not help discriminating amongst allowed spectral functions.

V. THE AVERAGE SPECTRUM METHOD

Given the weak discriminating nature of the prior, Eq. (7), it is not a good idea to follow the MaxEnt method and pick as the final answer the spectral function that maximizes the posterior probability distribution. It is rather obvious that the spectrum so obtained will over-fit the data in the sense that it also will fit the noise. This is avoided in the MaxEnt method where the entropic prior constrains the optimal solution to be smooth. Instead we will pick as the final answer the *average* spectral function, obtained by averaging over the posterior distribution⁵. Thus we will compute

$$\bar{A} = \int dA AP(A|G) / \int dAP(A|G). \quad (8)$$

The averaging procedure itself will protect against over-fitting the data. In a sense the averaging procedure takes the smoothing role of the entropic prior in the MaxEnt method, and, in fact, it has been shown that when the average is carried out within the mean field approximation the result is identical to the MaxEnt result¹⁰. However, in general the methods yield different results.

Taking the average as the final answer is appropriate when the posterior probability has a single prominent peak. However, when there are more peaks the meaning of the average becomes more questionable. In order to detect such multiple peak situations one can focus on a few spectral features and make histograms of these according to the posterior probability distribution, and check for multiple peaks in these histograms.

The averaging procedure can be efficiently carried out using Monte Carlo methods. In the context of getting dynamics from QMC this approach is known as the Average Spectrum Method⁵, or Stochastic continuation⁶, but it is also used for data analysis in many other fields, see for instance Refs. 11 and 12, where it is generally known as Markov Chain Monte Carlo methods.

To compute the posterior probability $P(A|G)$ we need the likelihood function $P(G|A)$. Assuming that the imaginary time data is distributed as Gaussians with covariance matrix Σ , the likelihood function $P(G|A)$ is

$$P(G|A) \sim e^{-\frac{1}{2}Tr \sum_i (\mathbf{G}^i - \mathbf{G}_A)^T \Sigma^{-1} (\mathbf{G}^i - \mathbf{G}_A)} \quad (9)$$

where we have denoted by \mathbf{G}^i a vector of imaginary time values G_τ^i that is the average result of the i 'th bin of QMC data containing M measurements. The assumption of having Gaussian data should be good for large amount of data, however this assumption should always be checked for instance by monitoring skewness and kurtosis. Similarly we denote by \mathbf{G}_A a vector with components

$$G_{A\tau} = \sum_j K_{\tau\omega_j} A_{\omega_j} \quad (10)$$

coming from a particular spectral function A_ω . In total there are n bins of QMC data, and for large n , Σ can be approximated by the measured covariance matrix having components

$$\Sigma_{kl} \approx \frac{1}{n-1} \sum_i (G_{\tau_k}^i - \bar{G}_{\tau_k}) (G_{\tau_l}^i - \bar{G}_{\tau_l}) \quad (11)$$

where we have denoted by an over-bar the total mean of the QMC data

$$\bar{\mathbf{G}} = \frac{1}{n} \sum_i \mathbf{G}^i. \quad (12)$$

It is useful to express the posterior probability in terms of this total mean. Using the cyclic property of the trace the exponent can be written as

$$\begin{aligned} \text{Tr} \Sigma^{-1} \sum_i (\mathbf{G}^i - \bar{\mathbf{G}} + \bar{\mathbf{G}} - \mathbf{G}_A) (\mathbf{G}^i - \bar{\mathbf{G}} + \bar{\mathbf{G}} - \mathbf{G}_A)^T \\ = \text{Tr} \Sigma^{-1} \sum_i (\mathbf{G}^i - \bar{\mathbf{G}}) (\mathbf{G}^i - \bar{\mathbf{G}})^T \\ + n \text{Tr} (\bar{\mathbf{G}} - \mathbf{G}_A)^T \Sigma^{-1} (\bar{\mathbf{G}} - \mathbf{G}_A). \end{aligned} \quad (13)$$

The first term is independent of the model A and contributes only to the normalization, thus

$$P(G|A) \propto e^{-\frac{1}{2}n \text{Tr} (\bar{\mathbf{G}} - \mathbf{G}_A)^T \Sigma^{-1} (\bar{\mathbf{G}} - \mathbf{G}_A)}. \quad (14)$$

Note the explicit factor of n which makes the distribution more peaked as it increases. Thus for more accurate QMC data (larger n) a spectral function that fits the data well becomes increasingly more likely than one that does not fit so well. This factor of n reflects the well known fact that the variance of the mean value is down by a factor $1/n$. The value of n is of course rather meaningless without also specifying the number of measurements N_{meas} in each QMC bin, which determines the magnitude of the components of Σ . However, for a fixed value of N_{meas} , Σ is largely independent of n , thus the explicit factor of n reflects accurately how the likelihood function sharpens up when more measurements of QMC data is made.

VI. MONTE CARLO IMPLEMENTATION

The task of sampling the posterior distribution can be done efficiently using a Monte Carlo simulation that samples the distribution $P(A)e^{-\alpha E(A)}$. $P(A)$ is the prior probability, and the energy $E(A)$ comes from the likelihood function and is

$$E(A) = \frac{1}{2}n \text{Tr} (\bar{\mathbf{G}} - \mathbf{G}_A)^T \Sigma^{-1} (\bar{\mathbf{G}} - \mathbf{G}_A), \quad (15)$$

and $\alpha = 1$.

In devising a Monte Carlo procedure one can choose the probability of accepting a new spectral function A' as

$$p(A \rightarrow A') = P(A') \min(1, e^{-\alpha(E(A') - E(A))}). \quad (16)$$

To implement the prior probability $P(A)$ according to Eq. (7) one starts with a spectral function that is positive everywhere and satisfies the sum rule. In subsequent Monte Carlo moves one simply does not accept spectral functions which violate the positivity and the sum rule. Thus $P(A)$ is unity for allowed spectral functions and zero otherwise. Typically a simulation is started with all spectral weight concentrated at one frequency. In a Monte Carlo move spectral weight is shared between neighboring frequencies in the following manner. First a pair of neighboring frequencies ω_i and ω_{i+1} are chosen at random, and the contribution to the zero-moment sum rule from the spectral weights at these frequencies are computed: $c_0 = A_{\omega_i} K_{0\omega_i} + A_{\omega_{i+1}} K_{0\omega_{i+1}}$. Then a random number r is selected in the interval $[-c_0, c_0]$, and new spectral weights

$$\begin{aligned} A'_{\omega_i} &= A_{\omega_i} + r K_{0\omega_{i+1}} / (K_{0\omega_i} + K_{0\omega_{i+1}}) \\ A'_{\omega_{i+1}} &= A_{\omega_{i+1}} - r K_{0\omega_i} / (K_{0\omega_i} + K_{0\omega_{i+1}}) \end{aligned} \quad (17)$$

are proposed. Note that the zero moment sum rule is unchanged as $A_{\omega_i} K_{0\omega_i} + A_{\omega_{i+1}} K_{0\omega_{i+1}} = A'_{\omega_i} K_{0\omega_i} + A'_{\omega_{i+1}} K_{0\omega_{i+1}}$. This proposed move is accepted with the probability specified in Eq. (16). In particular, if either of the A 's are negative the proposed move is rejected. Note that for detailed balance to hold in this scheme c_0 must not change in a Monte Carlo move. For closely spaced frequencies this Monte Carlo move gives good acceptance rates when it is combined with a parallel tempering scheme in which several simulations of the system is simultaneously carried out at different temperatures α and a swapping move between different temperature configurations is included. In order to optimize the list of temperatures we have used the scheme in Ref. 13 where the maximum movement of configurations from the highest to the lowest temperatures is achieved.

In Ref. 6 it was suggested that the entropy of the averaged spectrum be plotted vs. α and the final spectrum would be selected as the average at a value of α just before the entropy makes a final drop at high values of α . We do not adopt such a procedure here as we find it undesirable to have a procedure for selecting the spectral function that depends on properties of the spectral function itself. Even though a high value of α gives solutions close to the most probable one there are no guarantees that the correct spectrum will not have a low entropy as is the case if the spectrum is well approximated by a single or a few narrow peaks. A similar criterion was proposed in Ref. 10 where the value of α corresponding to a jump in the specific heat was chosen.

In this article we instead take the point of view that the final answer is the average spectrum at $\alpha = 1$, which corresponds to the posterior distribution⁵. This means

that the resulting spectrum will depend on the accuracy of the input data, n . This is advantageous as it provides a mechanism against over-interpreting low quality data. However, it also means that one needs to monitor how larger values of n will influence the final result. Thus a convergence analysis with n is required. This makes the method rather dependent on efficient QMC algorithms as generally large values of n are needed.

VII. APPLICATIONS

For neutron scattering the relevant measured quantity is the dynamic structure factor

$$S_q^{ij}(\omega) = \int_{-\infty}^{\infty} dt e^{i\omega t} \langle S_q^i(t) S_{-q}^j(0) \rangle \quad (18)$$

where the superscripts i, j indicate polarization directions being either x, y or z , and $S_q^i(t)$ is the i 'th component of the spin operator in the Heisenberg representation at momentum q . For convenience we will choose units such that the lattice spacing is unity. In QMC the convenient correlation function to measure is the imaginary time correlation function

$$\tilde{S}_q^{ij}(\tau) = \langle S_q^i(\tau) S_{-q}^j(0) \rangle. \quad (19)$$

Using the Lehmann representation one finds that S^{ij} and \tilde{S}^{ij} are related by

$$\tilde{S}_q^{ij}(\tau) = \int_0^{\infty} \frac{d\omega}{2\pi} \left(e^{-\omega\tau} + e^{-(\beta-\tau)\omega} \right) S_q^{ij}(\omega), \quad (20)$$

where β is the inverse temperature. Thus the kernel $K_{\tau\omega}$ in Eq. (3) is

$$K_{\tau\omega} = \begin{cases} \frac{1}{2\pi} & , \omega = 0 \\ \frac{1}{2\pi} (e^{-\omega\tau} + e^{-(\beta-\tau)\omega}) & , \omega \neq 0. \end{cases} \quad (21)$$

A. Antiferromagnetic dimer in a magnetic field

In order to test the Average Spectrum Method for finding the spectral function we do a test on a simple system with a non-trivial spectrum. It is well known that the MaxEnt method has a hard time resolving peaks that are close together. Therefore we test the method on a system with two peaks. We choose the Hamiltonian of two spins in a magnetic field B

$$H = J \vec{S}_1 \cdot \vec{S}_2 - B(S_1^z + S_2^z). \quad (22)$$

The dynamic structure factor of the transverse field components $S_{\pi}^{xx}(\omega)$ is nontrivial and displays delta-function peaks at $\omega = J \pm B$ each of weight $\pi/[4(1 + e^{-\beta J}(1 + 2 \cosh \beta B))]$ which becomes $\pi/4$ at low temperatures.

We simulated the two-spin Hamiltonian at an inverse temperature $\beta J = 10$ using the stochastic series expansion QMC method¹⁴ with directed loop updates¹⁵. In the

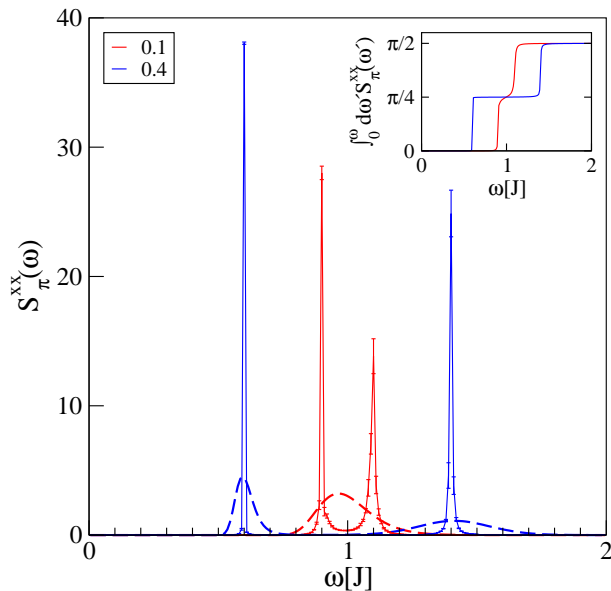


FIG. 1: (Color online) Real-frequency dynamic structure factor $S_{\pi}^{xx}(\omega)$ obtained from stochastic continuation (solid lines) and classic MaxEnt (dashed lines) for the two-spin Hamiltonian. The red(blue) curves are for a magnetic field value $B/J = 0.1(0.4)$. The inset shows the integrated spectrum for the two curves.

simulations we extracted the imaginary time correlation function in the x -direction at momentum vector π . The imaginary time data were obtained on an equally spaced grid with 101 points from 0 to $\beta/2$, and the relative error of the imaginary time data ranged from $\sim 10^{-5}$ at small τ to $\sim 10^{-2}$ at $\tau = \beta/2$. The imaginary time data was then used as input to the sampling program where we used a regular grid with 200 frequencies having spacing $\Delta\omega = 0.01J$.

The results for two values of the magnetic field $B/J = 0.1$ and 0.4 are shown in Fig. 1. As expected the Average Spectrum Method gives much sharper peaks than the MaxEnt solutions using a flat prior shown as dashed curves. The Average Spectrum Method is also capable of resolving the two peaks at $B = 0.1J$ while the MaxEnt solution gives a single broad asymmetric peak. For $B = 0.4J$ both methods are able to predict the location of the peaks, but MaxEnt gives much broader peaks.

While the Average Spectrum Method gives sharp peaks, they are not equal as dictated by the exact solution. There is a tendency that the high energy peak is lower and broader than the low energy peak. However, the spectral weight is equally distributed on the two peaks in both the low and the high field cases, see inset of Fig. 1. We expect that the peaks become more and more equal as the quality of the QMC data is increased (larger n). This has the effect that the likelihood function becomes more peaked and more details of the spectrum will be better resolved. An example of this is shown in Fig. 2 where it is clear the the double peak

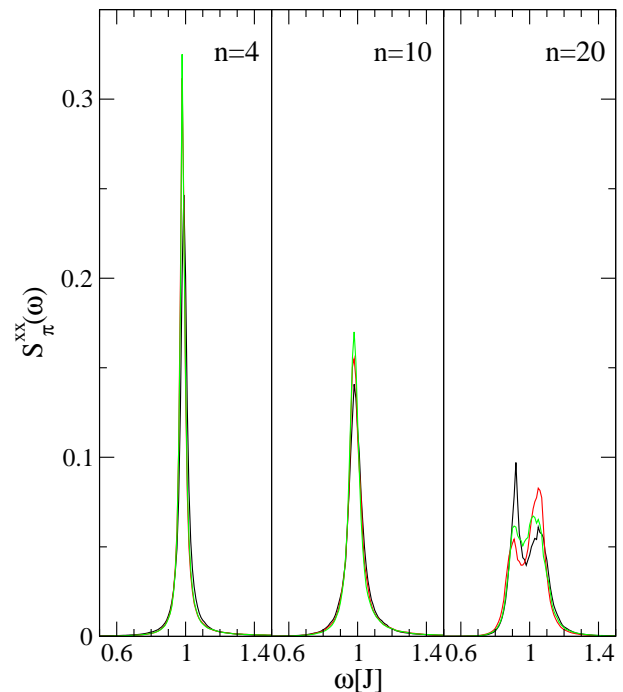


FIG. 2: (Color online) The effect of improving the data quality by increasing the number of Monte Carlo bins n . Each panel shows the dynamic structure factor for $B = 0.1J$ for three independent data set (different colors). The number of data bins were $n = 4$ (left), $n = 10$ (middle), and $n = 20$ (right). For comparison the results shown in Fig. 1 was carried out using $n = 200$.

structure is only revealed for data of sufficient quality.

B. Spin-1 chain

We now move to a nontrivial example, the spin-1 antiferromagnetic chain, the so called Haldane chain. The Haldane chain is famous for being gapped in contrast to the half-integer spin chains¹⁶. The minimum gap is at $Q = \pi$ in units of the inverse lattice spacing. Fig. 3 shows plots of $S_{Q=\pi}^{zz}(\omega)$ for different temperatures obtained using the Average Spectrum Method. Note how the peak position and width increase with temperature. To compare with MaxEnt we have shown the MaxEnt result for a single temperature $T/J = 0.125$ as a dashed curve. Note that the MaxEnt curve captures the peak position well, but gives a very broad peak. The inset shows a comparison of the temperature dependence of the gap vs. a non-linear sigma model prediction which was obtained by solving the finite temperature gap equation in Ref. 17 numerically. In the inset we also show a comparison of the width of the peaks, quantified by their full width at half maximum (FWHM), with predicted values from a combined nonlinear σ -model and scattering matrix calculation¹⁸. The agreement is quite remarkable and involves no adjustable parameters.

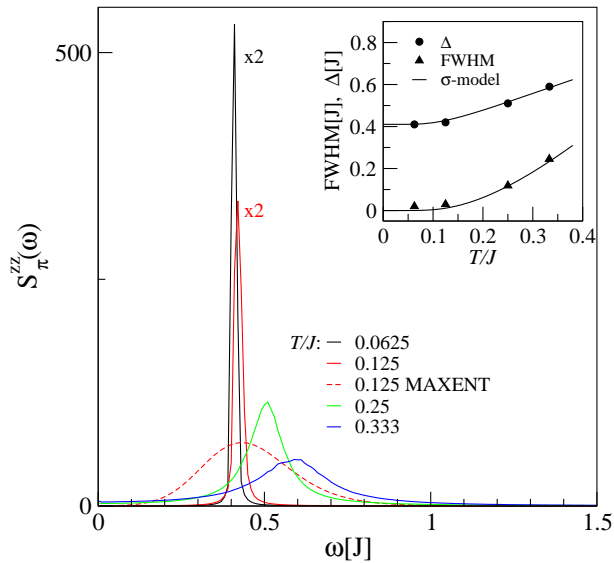


FIG. 3: (Color online) Dynamic structure factor $S_{\pi}^{zz}(\omega)$ for a 1D spin chain with 64 sites obtained from the Average Spectrum Method (solid lines) at different temperatures indicated by the legends. The dashed curve is the MaxEnt result for $T/J = 0.125$. The curves for $T/J = 0.0625$ and $T/J = 0.125$ have been scaled down by a factor 1/2 to fit inside the figure boundaries. The inset shows the peak positions Δ (circles) and peak widths FWHM (triangles) as functions of temperature. The solid lines are the σ -model predictions for these quantities.

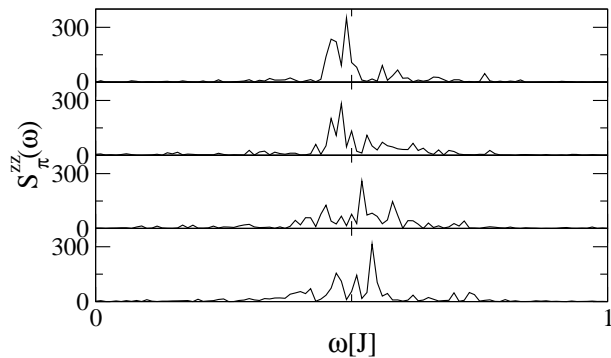


FIG. 4: Snapshots of spectra. These spectra (and others) are averaged over in order to yield the result shown in Fig. 3. The spectra here are all for $T/J = 0.25$.

One can ask whether the temperature broadening of the peak seen in Fig. 3 obtained using the Average Spectrum Method is just due to the “motion” of a single sharp peak. Fig. 4 shows that this is not the case.

C. Bond alternating antiferromagnetic chain

Another nontrivial spin model is the bond alternating spin-1/2 Heisenberg chain (BAHC) which has been studied extensively, and is relevant for materials such as

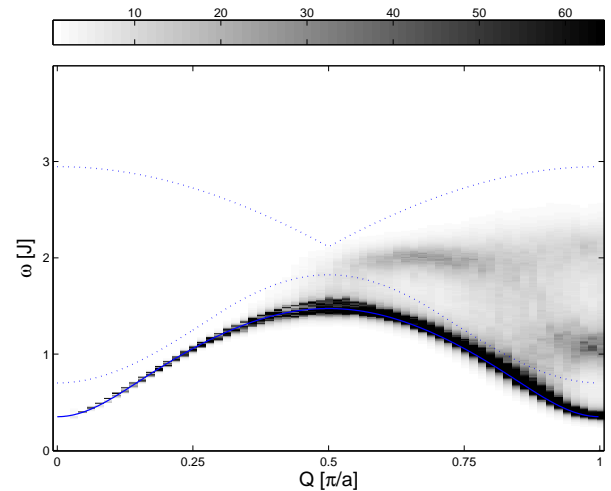


FIG. 5: Gray scale plot of $S_Q^{zz}(\omega)$ for the BAHC with $\lambda = 0.8$. The simulations were carried out at $\beta J = 16$ on a lattice with 128 sites and periodic boundary conditions. The solid blue curve indicates the one-magnon excitations as calculated using a series expansion about the dimer limit²², and the dotted lines show the kinematic boundaries of two-particle excitations.

$\text{Cu}(\text{NO}_3)_2 \cdot 2.5\text{D}_2\text{O}$ ^{19,20,21} and others (See Ref.²²). The Hamiltonian for the BAHC is

$$H = J \sum_i \left(\vec{S}_{2i-1} \cdot \vec{S}_{2i} + \lambda \vec{S}_{2i} \cdot \vec{S}_{2i+1} \right) \quad (23)$$

where $\lambda \geq 0$. Although the BAHC is a one-dimensional model, it is not solvable by the Bethe Ansatz. Thus other techniques are needed to obtain the dynamics. In this regard investigations using bosonization²³ the RPA approximation²⁴, series expansions^{22,25,26,27,28} and exact diagonalization studies²⁹ have produced very impressive results for the dynamics of the BAHC containing predictions of the dispersion of one magnon excitations as well as bound states and details about multi particle excitations.

We carried out QMC simulations of the BAHC for a chain with 128 sites and periodic boundary conditions at inverse temperature $\beta J = 16$ and $\lambda = 0.8$. The Average Spectrum Method was used to obtain the spectra at all momentum points. Figure 5 shows a gray scale plot of $S_Q^{zz}(\omega)$ for different values of Q and ω . The one magnon excitations are easily identified as the sharp dark feature and agrees very well with that obtained from series expansion to order λ^5 ,²² shown as the blue solid curve. For $Q \gtrsim 0.5\pi$ many-particle excitations are visible. This agrees qualitatively with the results in Ref. 28 which shows that the many-particle continuum has appreciably more spectral weight for $Q \gtrsim 0.5\pi$ than for smaller Q . For $0.5\pi \lesssim Q \lesssim 0.75\pi$ there is an almost flat feature in the continuum at $\omega \sim 1.9J$ which is well separated from the band of one magnon excitations and also from the kinematic boundaries of two magnon excitations shown as blue dotted lines. This is not seen from the se-

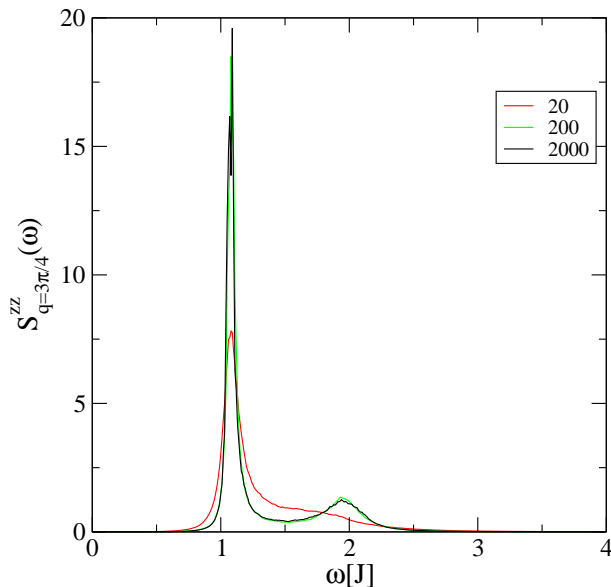


FIG. 6: Line shapes at a fixed momentum $Q = 3\pi/4$ for QMC data sets of different lengths n indicated by the legends.

ries expansion²⁸ and RPA results²⁴ which predict that the continuum should have biggest spectral weight at its lower boundary. However, this feature is reminiscent of that seen in experiments on $\text{Cu}(\text{NO}_3)_2 \cdot 2.5\text{D}_2\text{O}$ ²¹ where a dispersion-less feature in the continuum was reported. As Q is increased towards π this feature broadens and vanishes. Some structure reappears in the continuum close to $Q = \pi$ where a peak at $\omega \sim J$ and a very weak feature at $\omega \sim 2J$ is seen. A word of caution is needed in interpreting weak features of Fig. 5. This is because Fig. 5 shows occurrence of spectral weight in between the one magnon peak and the lower kinematic boundary of the two magnon excitations, where one expects a gap. This is probably caused by insufficient quality of the QMC data which gives spectral weight in unwanted places in a similar fashion to what is seen in Fig. 1 at $\omega \sim J$ for $B = 0.1J$.

The QMC data plotted in Fig. 5 were taken from a run with in all $n = 2000$ data bins. In order to see how the number of QMC bins affect the line shapes we show in Fig. 6 the dynamic structure factor at $Q = 3\pi/4$ for three different values of n . While there is some significant change in the line shape from $n = 20$ to $n = 200$, increasing n to 2000 has only minor effects.

We will now add a magnetic field term $-B \sum_i S_i^Z$ to Eq. (23). For $\lambda = 0$ the BAHC is just a collection of independent antiferromagnetic dimers. When subjecting a dimer to a magnetic field in the spin z direction the degeneracy of the spin triplet excitations is lifted, and one expects a double-peak structure, as seen in Fig. 1, in the transverse dynamic structure factor S^{xx} . For finite λ the dimers become coupled, however one still expects the splitting to occur, at least for small values of the magnetic field. Fig. 7 shows a gray scale plot of $S_Q^{xx}(\omega)$ for

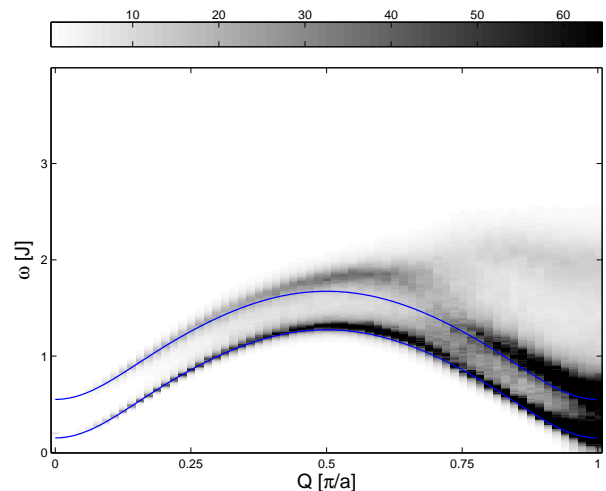


FIG. 7: Gray scale plot of $S_Q^{xx}(\omega)$ for the BAHC with $\lambda = 0.8$ in a magnetic field $B = 0.2J$. The inverse temperature is $\beta J = 16$ and $L = 128$. The solid lines are the spin-split one magnon result.

$\lambda = 0.8$ and a small value of the magnetic field $B = 0.2J$. The splitting of the one magnon peak is clearly seen and agrees, for small values of Q , well with the expectation that the effect of the magnetic field is simply to displace the one magnon dispersion by $\pm B$. The solid lines indicate this. We have taken the one magnon dispersion from the series expansion²² and added(subtracted) an energy $B = 0.2J$. For $0.5\pi \lesssim Q \lesssim 0.75\pi$ there are deviations from this simple picture, as the upper branch is higher in energy and broadens considerably. For even higher momentum values there is significant broadening of the peaks and at $Q = \pi$ they are hardly distinguishable. For $Q \gtrsim 0.75\pi$ one can also see the appearance of many-particle excitations above the one magnon peaks.

For a large value of the magnetic field the lower branch goes to zero energy at a certain characteristic value of the momentum. Figure 8 shows a gray scale plot of the transverse structure factor $S_Q^{xx}(\omega)$ for $\lambda = 0.8$ and $B = J$. One can clearly see that there is a branch of excitations that approaches zero at $Q \approx 0.3\pi$ and at $Q = \pi$. This is consistent with the results reported in Ref. 30. It is also apparent that the intensity at $Q \approx 0.3\pi$ vanishes as the energy approaches zero, while the intensity at $Q = \pi$ is high. The high energy magnon branch is clearly seen for $Q \lesssim 0.6\pi$ and gets broadened considerably and disappears for larger Q . There is also a sharp finite energy peak seen at small Q resulting from the merger of the two magnon branches.

D. Square lattice Heisenberg antiferromagnet

The spin-1/2 Heisenberg antiferromagnet on a square lattice (2DAF) has been studied intensively because of its relevance to the cuprate materials that are super-

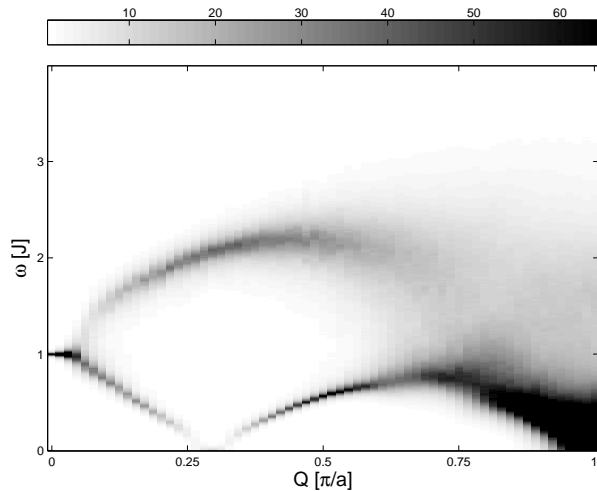


FIG. 8: Gray scale plot of $S^{xx}(Q, \omega)$ for the BAHC in a magnetic field $B = J$. $\lambda = 0.8$, $\beta J = 16$ and $L = 128$.

conducting at high temperatures when doped. The dynamics of the 2DAF is rather well described by linear spin-wave theory³¹. However, linear spin wave theory does not account for a magnon dispersion along the zone boundary. Such a dispersion was predicted using an expansion around the Ising limit^{32,33} and indicates a difference in energy between the magnon peaks at $(\pi, 0)$ and $(\pi/2, \pi/2)$ of about 7-9%, the energy at $(\pi/2, \pi/2)$ being the highest. Similar result was obtained using QMC: In Ref. 34 the QMC data were fitted to a functional form consisting of a delta-function and a broad continuum, while in Ref. 35 the MaxEnt method was used. Higher order Holstein-Primakoff spin wave calculations gives a smaller value, 2%³⁶, as does an expansion based on the Dyson-Maleev transformation^{37,38}.

Experimental measurements of the material copper formate tetradeuterate (CFTD)^{39,40} indicated a difference of 7% in agreement with the series expansion results and the QMC, however La_2CuO_4 shows⁴¹ an entirely different dispersion with the peak at $(\pi, 0)$ being higher in energy than at $(\pi/2, \pi/2)$. This dispersion has been explained as special features of the Hubbard model⁴². Recently experiments on $\text{K}_2\text{V}_3\text{O}_8$, also supposedly a realization of the Heisenberg antiferromagnet on the square lattice, showed a double peak structure of unknown origin at $(\pi/2, \pi/2)$ ⁴³. In order to investigate this possible double peak structure we repeated the simulations of Ref. 34 and analyzed the imaginary time data using the Average Spectrum Method which gives unbiased information about the line shapes. In order to distinguish transversal and longitudinal excitations the simulations were carried out as in Ref. 34 by imposing a staggered magnetic field $H_{\text{stag}} = 0.001615$ that yields a staggered magnetization consistent with the experimental value $m_s = 0.307$ on a 32×32 lattice at an inverse temperature $\beta J = 32$. We measured both the transverse dynamic structure factor S^{xx} and the longitudinal one

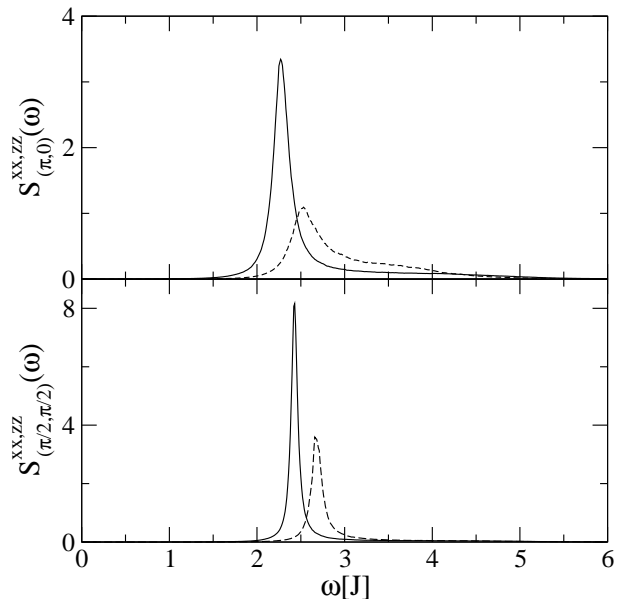


FIG. 9: Transverse (solid curves) and longitudinal (dashed curves) dynamic structure factor for the 2DAF at $Q = (\pi, 0)$ (upper panel) and $Q = (\pi/2, \pi/2)$ (lower panel).

S^{zz} . The results for the two momentum points $Q = (\pi, 0)$ and $Q = (\pi/2, \pi/2)$ are shown in Fig. 9. We observe a difference in magnon energies in the transverse channel corresponding to $(E_{(\pi/2, \pi/2)} - E_{(\pi, 0)})/E_{(\pi/2, \pi/2)} \approx 6\%$, determined from the location of the maximum. However, the peak locations are at slightly higher energies than the corresponding delta-function locations found in Ref.34. As we expect a priori that the dynamic structure factor in the transverse channel contains a delta-function like one magnon peak and a continuum we believe that the result in Ref. 34 is the most accurate as it accounts for more prior information. However, for the longitudinal channel the expected functional form of the spectral function is not so clear. In particular it is not obvious that the particular functional form chosen in Ref. 34 in the longitudinal channel is flexible enough to track the real line shape. In fact, in contrast to the result reported there, at $Q = (\pi/2, \pi/2)$, the lower panel of Fig. 9 shows that the peak location in the transverse channel is at a substantial lower energy ($\sim 10\%$) than the peak in the longitudinal channel. For an experiment that measures both the longitudinal and transverse structure factors simultaneously this could give rise to a double peak structure at $(\pi/2, \pi/2)$. Such a double peak should also be apparent at $(\pi, 0)$, although more weakly, because the longitudinal structure factor is more strongly peaked at $(\pi/2, \pi/2)$ than at $(\pi, 0)$. In fact, as can be seen from Fig. 9 the longitudinal dynamic structure factor at $(\pi, 0)$ has a very long high-energy tail.

VIII. SUMMARY

Obtaining equilibrium dynamics from numerical imaginary time correlation functions is an important task. The most popular method for carrying out this task is the MaxEnt method. However, the MaxEnt method gives unduly smooth spectral functions because of its use of the entropic prior. The use of the entropic prior is commonly justified by either an assumption of the existence of finite discrete units of spectral weight or by an interpretation of the spectral function as a probability distribution in one variable. We find neither of these assumptions reasonable nor convincing.

Instead we argue for the use of a less constraining prior that just encodes hard knowledge; spectral positivity and sum rules. This prior probability distribution is combined with the likelihood function of the data into a posterior distribution which is sampled using a classical Monte Carlo simulation and the average result is collected. This sampling method is known as the Average Spectrum Method⁵. It is also in essence identical to the Stochastic continuation method⁶, except for the fact that the notion of a drop in entropy as the criterion for determining the temperature at which the sampling is carried out is not employed. Instead the posterior probability distribution is sampled directly. Thus in essence the quality of the input data determines the effective sampling temperature which is implicit in our approach. We find this desirable as it protects from over interpreting bad data and makes the procedure independent of the particular form of the spectral function itself. However, this also implies the need of a convergence analysis of the obtained spectral function with increasingly better QMC data. The Average Spectrum Method is on at least as firm statistical footings as the MaxEnt method, and while it is more computationally demanding than the MaxEnt method, it is not as computer-intensive as the QMC simulations themselves.

In showing examples of the Average Spectrum Method we have sampled the posterior probability distribution

and obtained spectral functions for several model systems. Of new results we have shown that using this method we can obtain the finite temperature position and broadening of the Haldane gap in spin-1 antiferromagnets, and that the results agree very well with nonlinear σ -model predictions without any adjustable parameters. We have also applied the method to the spin-1/2 Heisenberg chain with alternating bond strengths where we found a quantitative very good agreement with other methods for the dispersion of one magnon excitations. We also observed some structure in the continuum of many-particle excitations which have not been seen using other methods. At present it is unclear whether these many-particle features are real or whether they are artifacts of insufficient QMC data. We have also added a magnetic field to the bond alternating chain, and observed the expected spin-split spectrum in the transverse dynamic structure factor. For a bigger value of the magnetic field we also see the weak incommensurate low-energy mode and the much stronger low-energy mode at $Q = \pi$. Finally we studied the dynamic structure factor at the zone boundary for the two dimensional square lattice spin-1/2 Heisenberg antiferromagnet, and found results consistent with existing results on that system except for a difference in peak locations of the transverse and longitudinal dynamic structure factor at the same momentum value that can possibly give rise to a double peak structure in measurements using unpolarized neutrons.

Acknowledgments

The author thanks Anders Sandvik for introducing him to the Stochastic continuation method and for making him aware of Ref. 5. The numerical simulations were in part carried out using the Nordugrid ARC middleware on SWEGRID computers provided by the Swedish National Infrastructure for Computing under the contract SNIC 021/06-64.

¹ C. E. Shannon, Bell Systems Tech. J. **27**, 379 (1948).

² E. T. Jaynes, "Probability Theory: The Logic of Science", Ed. G. Larry Bretthorst, Cambridge (2003).

³ R. N. Silver, D. S. Sivia, and J. E. Gubernatis, Phys. Rev. B **41**, 2380 (1990).

⁴ M. Jarrell and J. E. Gubernatis, Phys. Rep. **269**, 133 (1996).

⁵ S. R. White, in *Computer Simulation Studies in Condensed Matter Physics III*, Edited by D. P. Landau, K. K. Mon, and H. -B. Schuttler, (Springer-Verlag Berlin, Heidelberg 1991).

⁶ A. W. Sandvik, Phys. Rev. B **57**, 10287 (1998).

⁷ S. F. Gull and G. J. Daniel, Nature **272**, 686 (1978)

⁸ E. T. Jaynes, "Monkeys, Kangaroos, and N" in "Maximum Entropy and Bayesian Methods in Applied Statistics", eq. J. H. Justice, Cambridge (1986).

⁹ S. F. Gull and J. Skilling, IEE Proc. **131**, 646 (1984).

¹⁰ K. S. D. Beach, arXiv:cond-mat/0403055.

¹¹ K. Mosegaard and A. Tarantola, Jour. of Geophysical Research **100**, B7, 12431 (1995).

¹² A. J. Drummond, G. K. Nicholls, A. G. Rodrigo and W. Solomon Genetics **161**, 1307-1320 (2002).

¹³ H. G. Katzgraber, S. Trebst, D. A. Huse, and M. Troyer, J. Stat. Mech. P03018 (2006).

¹⁴ A. W. Sandvik and J. Kurkijärvi, Phys. Rev. B **43**, 5950 (1991)

¹⁵ O. F. Syljuåsen and A. W. Sandvik, Phys. Rev. E **66**, 046701 (2002).

¹⁶ F. D. M. Haldane, Phys. Lett. A **93**, 464 (1983).

¹⁷ Th. Jolicœur and O. Golinelli, Phys. Rev. B **50**, 9265 (1994).

¹⁸ K. Damle and S. Sachdev, Phys. Rev. B **57**, 8307 (1998).

- ¹⁹ L. Berger, S. A. Friedberg, and J. T. Schriempf, *Phys. Rev.* **132**, 1057 (1963).
- ²⁰ G. Xu, C. Broholm, D. H. Reich, and M. A. Adams, *Phys. Rev. Lett.* **84**, 4465 (2000).
- ²¹ D. A. Tennant, C. Broholm, D. H. Reich, S. E. Nagler, G. E. Granroth, T. Barnes, K. Damle, G. Xu, Y. Chen and B. C. Sales, *Phys. Rev. B* **67**, 054414 (2003).
- ²² T. Barnes, J. Riera, and D. A. Tennant, *Phys. Rev. B* **59**, 11384 (1999).
- ²³ A. M. Tsvelik, *Phys. Rev. B* **45**, 486 (1992).
- ²⁴ G. S. Uhrig and H. J. Schulz, *Phys. Rev. B* **54**, R9624 (1996).
- ²⁵ M. Gelfand and R. R. P. Singh, *Adv. Phys.* **49**, 93 (2000).
- ²⁶ S. Trebst, H. Monien, C. J. Hamer, Z. Weihong, and R. R. P. Singh, *Phys. Rev. Lett.* **85**, 4373 (2000).
- ²⁷ C. J. Hamer, W. Zheng and R. R. P. Singh, *Phys. Rev. B* **68**, 214408 (2003).
- ²⁸ R. R. P. Singh, W. Zheng, and C. J. Hamer, *Physica B* 385-386, 313 (2006).
- ²⁹ H. J. Mikeska and C. Luckmann, *Phys. Rev. B* **73**, 184426 (2006).
- ³⁰ R. Chitra and T. Giamarchi, *Phys. Rev. B* **55** 5816 (1997).
- ³¹ P. W. Anderson, *Phys. Rev.* **86**, 694 (1952).
- ³² R. R. P. Singh and M. P. Gelfand, *Phys. Rev. B* **52**, R15695 (1995).
- ³³ W. Zheng, J. Oitmaa, and C. J. Hamer, *Phys. Rev. B* **71**, 184440 (2005).
- ³⁴ A. W. Sandvik and R. R.P. Singh, *Phys. Rev. Lett.* **86**, 528 (2001).
- ³⁵ O. F. Syljuåsen and H. M. Rønnow, *J. Phys. Condens. Matter* **12**, L405 (2000).
- ³⁶ J. I. Igarashi, T. Nagao, *Phys. Rev. B* **72**, 014403 (2005).
- ³⁷ C. M. Canali, S. M. Girvin, and M. Wallin, *Phys. Rev. B* **45**, 10131 (1992).
- ³⁸ C. M. Canali and M. Wallin, *Phys. Rev. B* **48**, 3264 (1993).
- ³⁹ H. M. Rønnow, D. F. McMorrow, R. Coldea, A. Harrison, I. D. Youngson, T. G. Perring, G. Aeppli, O. Syljuåsen, K. Lefmann, and C. Rischel, *Phys. Rev. Lett.* **87**, 037202 (2001).
- ⁴⁰ N. B. Christensen, D. F. McMorrow, H. M. Rønnow, A. Harrison, T. G. Perring, and R. Coldea, *J. Magn. Mater.* **272-276**, 896 (2004).
- ⁴¹ R. Coldea, S. M. Hayden, G. Aeppli, T. G. Perring, C. D. Frost, T. E. Mason, S.-W. Cheong, and Z. Fisk, *Phys. Rev. Lett.* **86**, 5377 (2001).
- ⁴² N. M. R. Peres and M. A. N. Araújo, *Phys. Rev. B* **65**, 132404 (2002).
- ⁴³ M. D. Lumsden, S. E. Nagler, B. C. Sales, D. A. Tennant, D. F. McMorrow, S.-H. Lee, and S. Park, *Phys. Rev. B* **74**, 214424 (2006).